IRAS pointed observations data processing

Assendorp, R; Wesselius, PR

Published in:
Astronomy & astrophysics supplement series

Publication date:
1993

ASTRONOMY & ASTROPHYSICS
SUPPLEMENT SERIES

Astron. Astrophys. Suppl. Ser. **100,** 473-488 (1993)

IRAS pointed observations data processing

R. Assendorp and P.R. Wesselius

Kapteyn Institute, PO Box 800, 9700 AV Groningen, The Netherlands

Received August 31; accepted December 10, 1992

Abstract. — We have developed a system to process raw IRAS Pointed Observation (PO) data, using software developed at the Laboratory for Space Research, Groningen, The Netherlands. Several PO's can be coadded into one image. As an example we processed 99 PO's in the Chamaeleon I molecular cloud into one image for every IRAS band. The list of extracted point sources contains some 300 new IRAS sources, down to a flux level of 21 mJy at 12 μm.

Key words: methods: data analysis — techniques: image processing — infrared: general

1. Introduction

The Infrared Astronomical Satellite (IRAS), launched in 1983 and operational for about 300 days, used roughly two thirds of its lifetime to make a broad band photometric survey of the sky at 12, 25, 60 and 100 μm. This resulted in the IRAS Point Source Catalog (IPSC, see IRAS Explanatory Supplement (IES), 1988) which contains about 250,000 infrared sources.

The remaining one third was used to carry out Pointed Observations (PO's) (see Sect. 2.1) of objects or regions of special interest. PO's can be classified into two major groups: (i) Survey Instrument PO's (Young et al. 1985), and (ii) Chopped Photometric Channel PO's (Wesselius et al. 1985). In this paper the term PO will refer to Survey Instrument PO's. There are more than 8500 PO's of which Young et al. processed slightly less than 7500 into images available in FITS (Wells et al., 1981) format. Some 3600 of these images have been analyzed by Kleinmann et al. to create the Serendipitous Survey Catalog (SSC, 1986).

Despite the large amount of PO's towards star formation regions, relatively few have been used scientifically. Young et al. (1986) report the coaddition of some PO's in the ρ Ophiuchi region. They detected 18 sources while the IPSC only detected 5. Assendorp et al. (1990) coadded images made by Young et al. (1985) to obtain high resolution maps of the reflection nebulosities CED111 and CED112 (Cederblad, 1946) in the Cha I star forming region. They detected fifteen sources of which three are not listed in the IPSC; for seven IPSC entries they could determine fluxes for more bands than listed in the IPSC. These papers show that the PO data is of good quality and very useful for the study of small regions. The only drawback of the PO's is the amount of work needed to process them into maps (see Sect. 3).

We used software developed at the Laboratory for Space Research Groningen, The Netherlands, described by Wesselius et al. (1992), to process raw PO data into images. The main differences between our system and the Young images are: (i) all the basic image parameters like e.g. pixel size are user definable, (ii) several PO's can be coadded into one map, and (iii) the system is incorporated into the Groningen Image Processing System (GIPSY, 1992), which provides the user with many general facilities for image handling and analysis.

This paper describes the PO's (Sect. 2.1), the PO data processing (Sect. 3.1), and a method to extract point sources (Sect. 3.2) from the images. In Sect. 4 the result of processing 99 PO's in the Chamaeleon I area is presented as an example. The analysis of the maps will be discussed separately.

Readers interested in the PO data and processing are invited to contact the authors. The complete data base of raw PO data is available at the Laboratory for Space Research and the facilities can be used by visitors.

2. Data

2.1. Pointed observations

A Pointed Observation was performed by IRAS in the following way. The satellite made a raster scan of a small region of sky consisting of parallel scans, 'legs', separated by a distance, 'cross step' (see Fig. 1). The satellite scanned adjacent legs in opposite direction. The length of a leg for various PO types varies from almost zero to 360 arcminutes and the cross step from zero to 28 arcminutes. For PO's, the scan speed of IRAS was often chosen to be lower than during the survey scans to increase the signal to noise ratio. The lowest speed used was one eighth of the survey scan speed ($\simeq 0'.5/s$). A table summarizing the characteristics of the various PO's can be found in Young et al. (1985, Table 2).

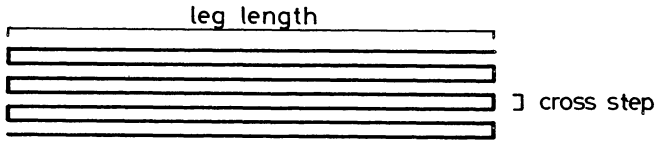

Fig. 1. Track of a typical PO. It consists of 7 legs

Several PO types, 'macro's', correspond to special scan patterns. E.g. the DSD01A macro was used for high spatial resolution mapping. It performed a scan pattern such that four of the small survey detectors at the edge of the focal plane (numbers 31, 39, 47 and 55) completely cover a $10' \times 10'$ area of the sky. This gives for the 12, 60 and 100 μm bands a good spatial resolution because the detectors used are small and almost square. For the 25 μm band, unfortunately, the cross-scan dimension of the detector is about three times its in-scan dimension. Because only the small detectors are used, the accuracy of the point source flux extracted from a DSD macro is poor with respect to the IPSC. Other macro's have scan patterns such that an area of sky is covered by many normal detectors, e.g. the DPP51C macro (14 legs, 0.2′ cross step), which has an expected gain in signal to noise ratio with respect to the IPSC of a factor of 10.

A number of working groups of the Joint IRAS Science Working Group (JISWG) prepared lists of interesting regions and objects to be observed with one or more PO's. In our sample we have PO's from the Molecular Cloud group, the Galactic Structure group, and some PO's that were originally carried out for calibration purposes.

In Table 2 of Young et al. the *intended* PO characteristics are listed, and the maps are a reflection of the original aim of the relevant macro. So, a DSD PO, processed by Young et al., resulted in a map that only contains information obtained by the small edge detectors mentioned. But, in fact all detector data was collected during a PO. Our system can make maps using any arbitrary detector combination. If, for a DSD PO, all large detectors are used, there will be some loss of spatial resolution but a considerable gain in sensitivity.

In Table 1 we present the characteristics of the PO's we used for the Chamaeleon maps. In the area of Cha I there are also some DPP macros, but since these macros have a scan length of almost zero, the detectors of one band do not cover a contiguous piece of sky and therefore the data is very hard to process. They were not used for the maps.

Table 1. Characteristics of PO's used for the maps. The scan speed is for all macro's 0.5 times the nominal survey speed. The column labeled '#' presents the number of legs, 'l' the length of a leg, 'cs' the cross step, and 'nr' the number of macros of the particular type in the Cha I area

Macro	#	l (′)	cs (′)	nr
DPS02B	6	96	0.3	42
DPS52B	6	96	0	14
DPS60D	5	48	0	12
DPS62D	9	96	0.4	6
DSD01A	18	28	0.5	25

3. Data processing

3.1. Imaging

We will discuss the special problems encountered when trying to process PO's. A full description of IRAS data processing, including the destriping routine, is presented by Wesselius et al. (1992).

The processing of IRAS data into maps consists of three basic steps: (i) calibrate to remove gain and offset differences between detectors and to convert the data to physical units, (ii) merge the calibrated data with the position information, and (iii) construct an image.

The original data consists of files containing all detector data for one band for one PO. The unit of this data is an uncalibrated voltage passed through an analogue to digital converter on board the satellite. For the calibration of voltage to MJy per sterad, we used software developed at the Infrared Processing and Analysis Center (IPAC), based on the internal calibrator and a detector behaviour model as described in IES, Sect. VI. IPAC has used the same calibration to produce most of its data products.

Because the raw data files do not contain pointing information, this is obtained from the Boresight Pointing History File (BPHF), a data product of IPAC which contains the pointing direction of IRAS for every second of its lifetime.

Initially all detectors (15 or 16 per band) have a different zero level which varies slowly with time. When they are simply coadded, the resulting map shows lots of stripes. We use a routine that simultaneously takes care of imaging and destriping. It can discriminate against non-celestial detector outputs and can remove linear baselines from scans before combining them into a map. The latter can only be done properly when there is sufficient overlap between the scans that ultimately form the map.

Two problems may arise when destriping PO's: (i) there is too little overlap to do a proper destriping, due to short legs, and (ii) sky background structures, larger than the leg of a PO, will be removed by the baseline fitting.

Both problems have satisfactorily been overcome. We have destriped the PO's with respect to a template survey map, created by processing IRAS survey scans into a map having a larger map area and the same pixel size as desired for the composite PO map. The survey scans have enough overlap to be properly destriped and they are long with respect to the extended structures.

We have applied this procedure to the PO's from the Chamaeleon-I molecular region. The results will be discussed in Sect. 4.1.

3.2. Source extraction

On of the main aims of analyzing PO maps is to extract point sources down to a lower flux level than is possible using the IRAS survey data. In this section we will discuss the procedure used for extracting sources and the compilation of a list of point source candidates. Subsequent reduction of this list, in order to enhance its reliability will be discussed in Sect. 4.2.

There are two basic methods for extracting sources from data consisting of multiple scans (as is the case with the IRAS data); (i) extract point source candidates from individual scans and confirm them using detections in other scans running over the same area of sky, and (ii) extract point sources from coadded data. The first method was used to compile the IPSC. A square-wave filter was applied to each detector data stream to detect point sources (see IES, Sect. V-C). Seconds, hours, and weeks confirmation of the detections were used to enhance the reliability. The second method was used for the IRAS Faint Source Survey (FSS) and is described in the FSS Explanatory Supplement (FSS-ES, 1989, Chap. II). The individual scans were coadded into a map, that was searched for local maxima consisting of a contiguous area of at least six pixels with signal to noise ratio (SNR) of larger than three and one pixel with a SNR of at least 4.5.

The first method will produce a reliable source list, but weak sources are not detected. Weak sources are detectable when the noise is decreased by averaging scans (method ii), but some of them will be spurious.

Theoretically, the best way to detect point sources in a map is to look for structures that resemble the point spread function. However, in maps constructed from scans with different scanning angles, using detectors that are rectangular, the point spread function is complicated and will depend on position (see e.g. FSS-ES, Fig. II.C.9). For most PO maps the sky coverage is irregular in the number of scans and the scan direction. Consequently every map pixel has its own point spread function depending on detector behaviour and orientation at that particular point in the map. Therefore we developed a method similar to the FSS source extractor: estimate the background level (B) and noise (N) and search the map for features that are local maxima and whose pixel value (PV) exceeds the background by more than a pre-defined level (e.g. $(PV\text{-}B)/N = 3$).

Determining the noise and background in PO maps is not a straightforward procedure due to (i) non-uniform coverage of the area by PO's (ranging from one to 50) which causes fluctuations in the noise, and (ii) intrinsic background variations because of changes in the dust column density and temperature. To overcome these problems we used partially overlapping subarea's of our maps: the size of a subarea is 100×100 pixels, the centre points are on a regular grid with 20 pixels spacing. For each subarea we determined the local background and noise using a histogram of the pixel values. The histogram for the full map and a typical histogram for a subarea is shown in Fig. 2. We defined the peak of the pixel value[1] histogram to represent the background value and its Full Width at Half Maximum (FWHM) to be an indication for the noise. Figure 2 illustrates that background and noise estimates using subareas will give a better sensitivity for the detection of point sources than using the full map estimates. We use rather large subareas because for areas smaller than 100×100 pixels the background and noise can not be determined properly. The overlap enables us to determine the background and noise in areas of 20×20 pixels, an area over which the background changes by only minute amounts, by averaging relevant numbers.

For every subarea a 'sublist' of point source candidates is extracted. The list contains pixel coordinates, pixel value, local background value and noise estimate for all pixels that (i) exceed the background by $(PV\text{-}B)/N > 3$, (ii) are a local maximum within an area of 10×10 pixels, and (iii) are at least 25 pixels from the edge of the map. This last criterion is used because near the edge of the map PO coverage decreases rapidly, giving an unpredictable increase in the noise figure.

Due to the overlap of the subareas, every real point source should, in principle, be listed in 25 sublists. In practice this only holds for strong point sources, weak point sources can be missed in several subareas due to background deviations from the average within a subarea. The choice of the number of sublists (N) in which a point source

[1]The dimension of pixel value is flux density, in units of MJy/sterad

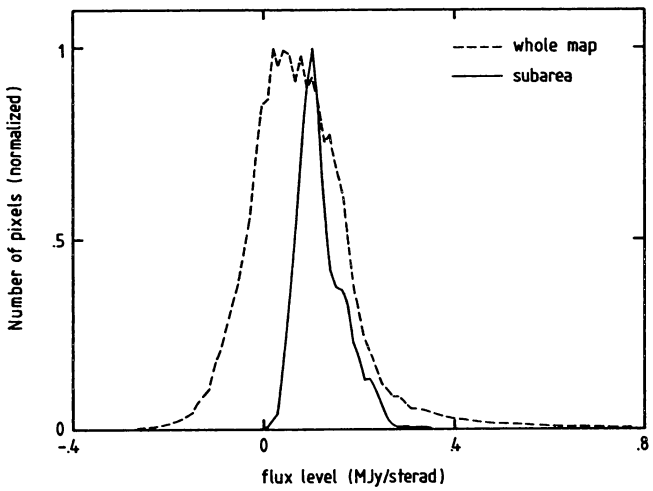

Fig. 2. Histogram of pixel values for the whole map and for a typical subarea

must occur in order to be considered 'detected' is rather arbitrary. In our example the number of 12 μm sources varies from 794 to 597 when N is 5 respectively 20. On the one hand we want to derive a reasonably reliable list of point sources, on the other hand we want to be as complete as possible. We have therefore chosen that N =10. Thus, the Raw Data Point Source List (RDPSL) contains all point sources that are detected in at least 10 subareas.

The reliability of the RDPSL can be enhanced by e.g. merging sources found at different wavelengths, or by confirming them with observations at other wavelengths.

4. Data products

4.1. The maps

The 99 PO's in the Chamaeleon-I area have been coadded and destriped as described above. The combined map is presented in Fig. 7. At 12 μm map we also constructed a noise map (see Fig. 8) with a pixel size of 200″. In Table 2 the characteristics for the maps are presented: pixel size, range of pixel values (in MJy/sterad), and range of noise level. Negative pixel values are an artifact of the destriping routine. The level of stripes still visible is less than 0.2 MJy/sr for all bands.

The bar-like structure in the 25 μm map near 11^h10^m, -77° 25′ is caused by detector hysteresis caused by the Infrared Nebula. Although one might expect spurious entries in the object list arising from this feature, this is hardly the case because of the two-dimensional nature of the extraction routine.

The angular resolution of the PO maps is of the same order as the FSS, due to the fact that no resolution enhancement routines have been used. A higher angular resolution can be achieved by using only the small IRAS detectors (detector numbers 11, 31, 39, 46, 47, 55, and 62 in ESP, Fig. II.C.6) to make a map, a method that has been used for CED111 and CED112 by Assendorp et al. (1990), and for CED110 by Prusti et al. (1991a). A better resolution for large detector maps can be attained by applying maximum entropy methods to the data.

Table 2. Characteristics of the maps. Presented are the pixel size in arcseconds (ps), the range in pixel value in MJy/sr (pv), and the range in noise in MJy/sr (σ)

band	ps	pv		σ	
		min	max	min	max
12μm	10	-0.7	49	<0.01	0.13
25μm	10	-0.6	159	<0.01	0.14
60μm	20	-1.1	278	0.01	0.18
100μm	40	-6.3	202	0.46	4.7

4.2. Source list

A more reliable source list is created out of the RDPSL by the following steps: (i) eliminate close doubles, (ii) merge sources at different wavelength, (iii) associate with other IRAS catalogues, and (iv) remove single-band detections with low SNR.

Although the area is at a high ecliptic latitude, the cross-scan direction did not vary much. Therefore, detections up to 5′ in the cross-scan direction (close doubles) may well be caused by the same source. Detections are merged when the cross-scan distance is less than 120″ and the intensities agree within 25 %.

Detections at different wavelength are considered to be caused by the same source when the distance is less than 120″.

The result of steps (i) and (ii) is the Candidate Point Source List (CPSL), containing 712 possible sources. In Table 3 a summary of the CPSL is given as the number of sources detected in various band combinations. Steps (iii) and (iv) are discussed in Sect. 4.3, and Sect. 4.4 respectively.

4.3. Other IRAS catalogues

The CPSL has been compared with the IPSC and the FSS. Although the IRAS Serendipitous Survey Catalog (SSC, Kleinmann et al. 1986) is based on the PO's as well, this catalogue is not used for comparison because a study by Prusti (1991b) showed that for this region, the SSC does not contain more sources than the FSS.

Detections within 120″ of a catalogue entry, having the same (within 25 %) fluxes are considered to be associated. From our list 53 sources could be associated with IPSC sources and 129 with FSS sources. Figure 3 gives a histogram of the distances between the sources in our map

Table 3. Number of sources in the CPSL. The column 'band' refers to the IRAS bands, e.g. 0 1 0 1 means detections in band 2 and 4

band				N
1	2	3	4	
1	0	0	0	292
0	1	0	0	178
1	1	0	0	156
0	0	1	0	17
1	0	1	0	6
0	1	1	0	15
1	1	1	0	36
0	0	0	1	4
1	0	0	1	1
0	1	0	1	1
1	1	0	1	1
0	0	1	1	1
1	0	1	1	0
0	1	1	1	0
1	1	1	1	4
		Total		712

and the associated IPSC and FSS sources. The histogram shows that the merging distance of 120″ is adequate.

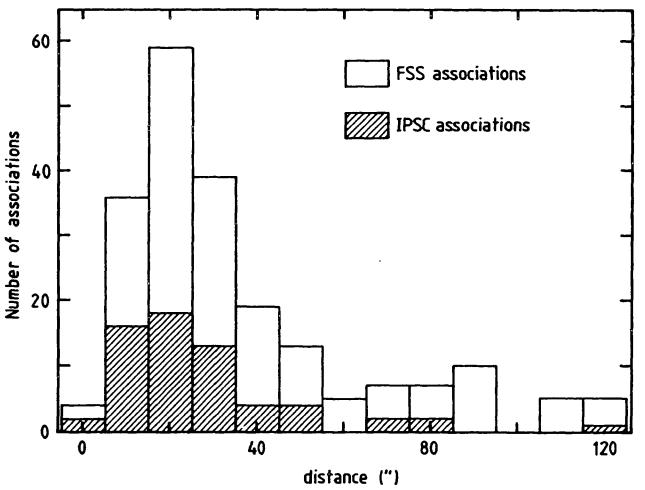

Fig. 3. Histogram of the distances between PO sources and the IPSC and FSS

There are a few IPSC and FSS sources that do not appear in our list. These objects can be classified into three groups. Those close to the edge of the PO map, those detected at 100 μm only, and those with uncertain detections in the FSS. Near the edge of our map, the number of PO's covering a certain region is low (it can be just one). These areas are very noisy and the source detections unreliable: real sources can be missed, and noise peaks can be noted as sources. The 100 μm only sources are probably cirrus features, listed in the IPSC and FSS as point sources, but not found by us as local maxima. The third group arises because we also used the FSS Reject File for this comparison. Detections in this file are less reliable and not included in the official release of the FSS.

Two objects, 11059-7721 (IPSC and FSS) and 11070-7725 (FSS), are good detections in the catalogues, but are not detected by our extraction routine. This is caused by the proximity of two very bright sources (HD97048 and IRN). These objects are embedded in the strong reflection nebula CED111 (Cederblad 1946). Assendorp et al. (1990) analysed PO's from the DSD type in this area using only small detector data. They detected the two objects and determined their flux.

The associated sources are listed in the Associated Source List (ASL, see Table 6).

4.4. Not-associated sources

The 578 sources in the CPSL that could not be associated with other IRAS catalogues are all weak detections with a SNR of typically less then 10. Sources that have only been detected in one band and have a SNR of less than 4 are unreliable, therefore we have removed them from the list.

This procedure removed most of the not-associated 100 μm detections from the list. We also removed the remaining 100 μm detections because at 100 μm there is lots of infrared cirrus. For these filamentary structures our flux calibration (see Sect. 4.5) does not give reliable numbers, and for the study of star formation they are of little interest.

The remaining sources are listed in the New Source List (NSL, see Table 7). A discussion and comparison of the ASL and NSL will be presented in Sect. 4.6.

4.5. Flux calibration

The flux of a point source can in principle be calculated by summing up all pixels that are influenced by the source and divide that number by the solid angle of the local point spread function. In practice this method is hampered by the same problems as the extraction of the point sources. Therefore we used the known fluxes of the ASL to fix our flux scale. Because the number of associations with the IPSC is quite low, we used the associations with the FSS. Figure 4 shows the peak pixel value of FSS sources in our 12 μm map versus the 12 μm FSS flux. The straight line is a least squares fit forced through the zero point.

Most of the sources to be calibrated are fainter than the ones listed in the FSS, and their fluxes are therefore derived by an extrapolation of the line fitted through the calibration points. Because the extrapolation is not so large, the faintest FSS source is 0.09 Jy at 12 μm and the faintest PO map object 0.012 Jy, it leads to reasonably reliable fluxes. For flux levels below 0.5 Jy we estimate that

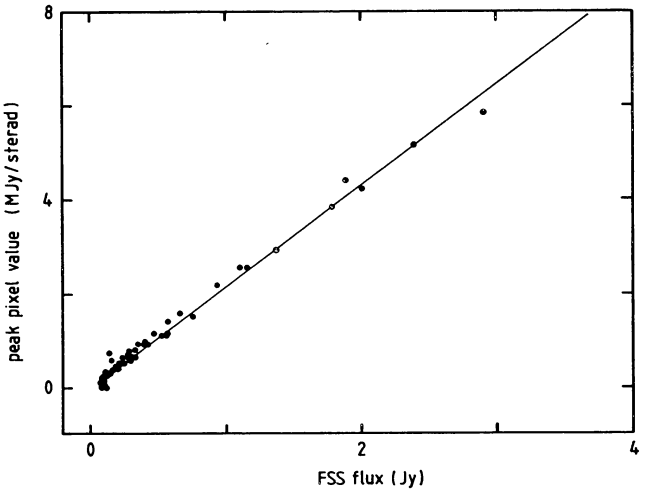

Fig. 4. The 12 μm calibration of PO sources, using the FSS flux scale

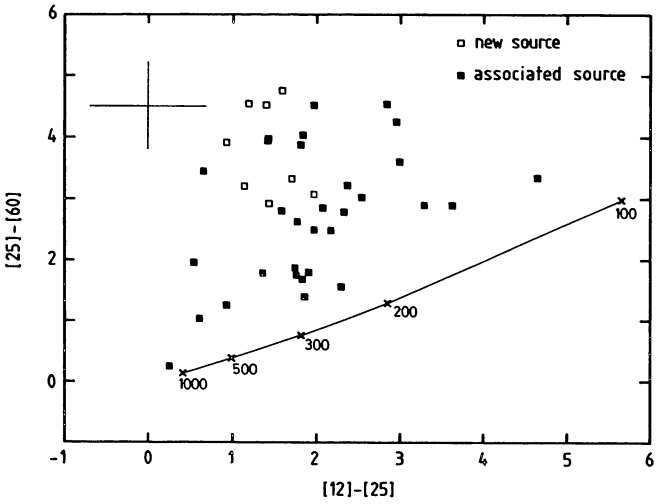

Fig. 5. Colour-colour plot of all sources with detection at 12, 25, and 60 μm

the uncertainty is about 30%. All brighter sources have fluxes listed in the FSS and/or IPSC.

The few points that do not match the fit can be understood as due to confusion (the flux estimate in the FSS and our intensity measure are not affected in the same way by nearby bright sources) or lack of coverage (in regions with low coverage the maximum pixel value is not a good flux measure).

Similar calibrations have been done for 25, and 60, the calibrations have been applied to our list of sources, and the values are incorporated in Tables 6 and 7.

4.6. Analysis of source lists

Various techniques have been applied to determine the reliability of both the ASL and NSL. For all sources with detections at 12, 25, and 60 μm a colour-colour plot has been made (see Fig. 5). The colours are calculated as defined by Walker et al. (1988). In the upper left corner error bars for a 30% error in the flux levels are shown. Most of the newly found sources are situated near the Young Stellar Object region of the colour-colour plot (Harris et al. 1988), which is in good agreement with the fact that the Chamaeleon cloud is a star forming region that contains many young objects.

For the 12 μm band a plot of the number of sources in a certain flux range versus that range is given in figure 6. The hatched parts designate the sample of associated sources. It is clear that all bright sources are associated with IPSC and/or FSS objects. For the 12 μm band most of the new sources are weaker than 230 mJy. This number is in good agreement with the completeness of the FSS as stated in the FSS-ES. From the histogram we may conclude that our 12 μm list is probably complete to 65 mJy. Our 25 μm list is complete to 40 mJy. A similar discussion for 60 μm is not possible due to the low amount of sources found in this band.

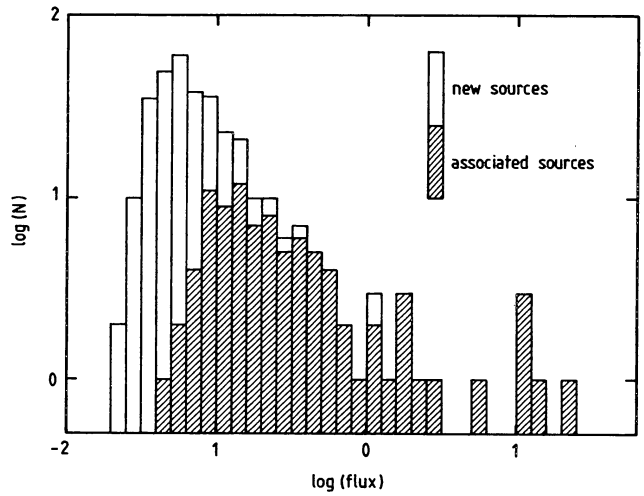

Fig. 6. Histogram of the number of sources for various flux levels

Table 4 presents a summary of the number of sources listed in the ASL and NSL. The entries in the NSL that are detected at 12 μm or at 12, and 25 μm tend to be situated in the areas of low extinction. We conclude that they are probably normal stars either in front of or next to the cloud.

The large number (64) of 25 μm only sources in the NSL is surprising. They can be real and caused by dust concentrations at a low temperature. If, e.g., the brightest 25 μm-only object has a temperature of about 100 K, its 12 μm flux is 10 mJy, just below the detection limit (see

Table 5). These objects need follow-up studies at other wavelengths to determine their reliability. This is beyond the scope of this paper. Another group of objects that need to be discussed are those that have been detected at 12, and 60 μm. These objects might be change coincidences of field stars and cirrus features.

There are many more entries in the NSL than in the ASL. This is because the NSL objects listed are less reliable, and it is probably a reflection of the normal luminosity function. There are more low luminosity sources than high luminosity sources, and the existing IRAS catalogues only detected the high luminosity sources.

Table 4. Number of sources detected in various band combinations in the ASL and NSL

band					
1	2	3	4	ASL	NSL
1	0	0	0	16	98
0	1	0	0	2	64
1	1	0	0	50	108
0	0	1	0	2	8
1	0	1	0	2	5
0	1	1	0	8	5
1	1	1	0	28	9
0	0	0	1	4	
1	0	0	1	3	
0	1	0	1	1	
1	1	0	1	4	
0	0	1	1	1	
1	0	1	1	0	
0	1	1	1	2	
1	1	1	1	11	
		Total		132	297

Table 5. A comparison of the faintest sources detected

	fluxes in mJy		
band	PO map	FSS	IPSC
12 μm	21	87	222
25 μm	23	114	314
60 μm	121	159	153

A comparison of the faintest objects detected in our 12, 25, and 60 μm maps and the IPSC and FSS entries in the region is tabulated in Table 5. It is clear that the best sensitivity can be obtained using the coadded PO data.

References

Assendorp R., Wesselius P.R., Whittet D.C.B., Prusti T., 1990, MNRAS 247, 624

Cederblad S., 1946, Medd. Lunds astr. Obs., Ser.II, No. 119

GIPSY User Guide, Kapteyn Astronomical Institute, Space Research Organization of the Netherlands, Expertise Centre Astronomical Image Processing, 1992

Kleinmann S.G., Cutri R.M., Young E.T., Low F.J., Gillet F.C. 1986, Explanatory supplement to the IRAS Serendipitous Survey Catalog (SSC)

Harris S., Clegg P.E., Hughes J., 1988, MNRAS 235, 441

(IES), Joint IRAS Science Working Group, 1988, Infrared Astronomical Satellite, Catalogs and Atlasses, Explanatory Supplement, eds. Beichman C.A., Neugebauer G., Habing H.J., Clegg P.E., Chester T.J.

(FSS-ES), Moshir M., Kopan G., Conrow T., McCallon H., Hacking P., Gregorich D., Rohrbach G., Melnyk M., Rice W., Fullmer L., White T., Chester T. 1989, Explanatory supplement to the IRAS Faint Source Survey , IPAC preprint 0044

Prusti T., Clark F.O., Whittet D.C.B., Laureijs R.J., Zhang C.Y., 1991a, MNRAS 251, 303

Prusti T. 1991b, private communication

Walker H.J., Cohen M., 1988, AnJ 95, 1801

Wells D.C., Greisen E.W., Harten R.H., 1981, A&AS 44, 363

Wesselius P.R., Beintema D.A., Jonge A.R.W., de Jurriens T.A., Kester D.J.M., Weerden J.E., van Vries J., de Perault M. 1985, IRAS-DAX Chopped Photometric Channel, Explanatory Supplement, Laboratory for Space Research Groningen

Wesselius P.R., Jonge A.R.W., de Kester D.J.M., Roelfsema P.R. 1992, in Infrared Astronomy with ISO, eds. Encrenaz, T., and Kessler, M.F., Nova Science Publishers Inc., New York

Young E.T, Neugebauer G., Kopan E.L., Benson R.D., Conrow T.P., Rice W.L., Gregorich D.T. 1985, A user's guide to IRAS pointed observation products

Young E.T., Lada C.J., Wilking B.A., 1986, ApJ 304, L45

Table 6. Associated Source List (ASL); sources in the PO map that could be associated with sources in the IPSC and FSS. The fluxes are in mJy, except for values labeled with *, which are in Jy. The column 'C' denotes the catalogue in which the flux is listed: P = PO map, F = FSS, and I = IPSC. The column 'SN' is the signal to noise ratio if the source is found in the PO map, otherwise it is the flux quality from the catalogue(s) mentioned in column 'C'

ra (1950)	dec	F1	SN	C	F2	SN	C	F3	SN	C	F4	SN	C
10:34:55	-77:11.0	120	3	F	64	3.8	P	-	-	-	-	-	-
10:36:25	-77:04.5	-	-	-	51	3.1	P	280	2	F	-	-	-
10:37:20	-77:02.5	-	-	-	75	4.1	PF	-	-	-	-	-	-
10:40:20	-76:54.5	36	3.3	P	65	2	F	-	-	-	-	-	-
10:43:15	-76:54.0	140	12.5	PF	-	-	-	-	-	-	-	-	-
10:43:30	-77:08.5	76	3.9	P	130	8.2	PF	870	2-3	FI	2.2*	3	I
10:43:55	-77:02.0	110	3	F	38	3.7	P	-	-	-	-	-	-
10:43:55	-76:59.0	200	15.1	PF	44	4.4	P	-	-	-	-	-	-
10:46:20	-77:45.0	-	-	-	79	2	F	700	6.5	PFI	2.5*	2	I
10:47:45	-77:41.0	-	-	-	-	-	-	250	3.6	PF	-	-	-
10:48:05	-76:39.5	140	12.8	PF	40	4.1	P	-	-	-	-	-	-
10:48:10	-76:51.0	-	-	-	-	-	-	220	4.0	PF	-	-	-
10:48:60	-77:44.0	55	4.8	P	-	-	-	160	2	F	-	-	-
10:49:25	-77:32.5	81	5.5	PF	56	3.3	P	-	-	-	-	-	-
10:49:55	-76:51.5	100	14.4	PF	30	3.1	P	-	-	-	-	-	-
10:50:30	-76:31.5	130	5.5	PF	-	-	-	-	-	-	-	-	-
10:51:05	-77:41.5	48	4.8	P	72	5.3	P	-	-	-	2.9*	2	F
10:51:05	-77:13.5	91	7.5	PF	-	-	-	-	-	-	-	-	-
10:51:15	-77:43.5	35	3.3	P	76	2	F	-	-	-	-	-	-
10:51:35	-77:20.0	53	3.8	P	-	-	-	-	-	-	3.0*	3	I
10:51:45	-77:14.5	50	4.0	P	-	-	-	-	-	-	5.9*	2	F
10:51:45	-77:60.0	130	10.4	PF	-	-	-	-	-	-	-	-	-
10:52:05	-77:26.0	87	5.0	PF	-	-	-	-	-	-	-	-	-
10:52:15	-77:02.0	26	3.2	P	34	3.1	P	-	-	-	2.8*	2	F
10:52:35	-76:56.5	-	-	-	72	4.3	PF	190	3.4	P	-	-	-
10:52:60	-76:38.5	2.8*	139.4	PFI	1.3*	74.8	PFI	-	-	-	-	-	-
10:53:40	-76:58.0	62	4.6	PF	47	3.5	P	-	-	-	-	-	-
10:54:30	-76:44.0	77	3.5	PF	-	-	-	-	-	-	-	-	-
10:54:40	-78:03.5	140	12.8	PF	46	3.2	P	-	-	-	-	-	-
10:54:50	-77:08.5	510	51.7	PFI	720	54.6	PFI	680	10.2	PFI	-	-	-
10:54:55	-77:37.0	230	19.6	PF	70	5.5	P	-	-	-	-	-	-
10:55:10	-77:29.0	320	27.6	PF	85	7.1	PF	-	-	-	-	-	-
10:55:20	-77:46.0	66	3.8	PF	29	3.6	P	-	-	-	-	-	-
10:55:20	-76:56.0	220	20.4	PF	500	32.0	PFI	480	4.7	PFI	-	-	-
10:56:30	-76:44.0	88	4.4	PF	150	7.9	PF	240	2	F	-	-	-
10:56:35	-78:15.0	42	3.0	P	71	4.1	P	-	-	-	3.2*	2	F
10:57:00	-77:22.0	37	4.6	P	48	4.5	P	320	5.7	PF	-	-	-
10:57:05	-77:01.5	250	23.9	PFI	1.3*	105.6	PFI	3.4*	38.7	PFI	3.4*	3	I
10:57:50	-77:07.0	210	30.7	PFI	370	39.3	PFI	450	3	I	-	-	-
10:57:50	-76:50.0	430	25.4	PFI	86	2	F	-	-	-	-	-	-
10:57:50	-76:46.0	1.2*	66.1	PFI	1.6*	93.4	PFI	1.2*	11.9	PFI	2.0*	2	I
10:58:40	-76:55.5	-	-	-	30	4.0	P	180	2	F	-	-	-
10:58:50	-78:07.0	98	5.9	PF	-	-	-	-	-	-	-	-	-
10:58:55	-76:28.5	280	31.0	PFI	140	14.4	PF	-	-	-	-	-	-
10:59:25	-77:46.0	320	23.9	PF	75	5.7	PF	-	-	-	-	-	-
10:59:35	-78:04.0	-	-	-	49	3.6	P	400	6.4	P	3.2*	2-3	FI
10:59:45	-77:23.0	49	3.5	PF	-	-	-	-	-	-	-	-	-
11:00:15	-77:28.0	31	3.3	P	71	5.4	PF	290	5.1	PF	-	-	-
11:01:10	-77:18.0	39	5.9	P	720	76.2	PFI	2.9*	50.9	PFI	-	-	-
11:01:35	-77:44.5	-	-	-	-	-	-	-	-	-	3.2*	2	F
11:02:10	-76:40.0	21	3.1	P	61	2	F	-	-	-	-	-	-
11:02:15	-77:25.0	140	13.2	PF	-	-	-	-	-	-	-	-	-
11:02:45	-76:23.5	52	6.9	P	77	9.0	PF	-	-	-	-	-	-
11:02:45	-76:36.0	120	18.4	PF	38	5.2	P	-	-	-	-	-	-
11:02:50	-76:11.5	760	46.4	PFI	920	56.7	PFI	740	25.5	PFI	-	-	-

Table 6. continued

ra (1950)	dec	F1	SN	C	F2	SN	C	F3	SN	C	F4	SN	C
11:03:05	-77:02.0	-	-	-	250	18.2	PFI	740	13.7	PFI	-	-	-
11:03:25	-77:26.0	41	4.0	P	70	2	F	-	-	-	-	-	-
11:03:30	-77:00.5	1.8*	108.1	PF	480	31.0	PF	-	-	-	-	-	-
11:03:45	-77:60.0	83	2	F	51	3.6	P	-	-	-	-	-	-
11:04:55	-77:06.0	330	20.8	PFI	140	3	F	9.1*	2	F	38*	2-2	FI
11:04:55	-77:54.0	110	8.4	PF	51	4.0	P	-	-	-	-	-	-
11:05:00	-76:17.5	150	3	F	120	6.2	PF	-	-	-	-	-	-
11:05:30	-77:07.0	560	29.5	PFI	1.8*	116.9	PFI	7.7*	194.0	P I	-	-	-
11:05:35	-76:57.5	200	12.4	PF	-	-	-	-	-	-	-	-	-
11:05:40	-77:10.5	130	8.4	PF	-	-	-	-	-	-	-	-	-
11:05:45	-76:16.5	96	6.0	PF	120	7.5	PF	-	-	-	-	-	-
11:05:45	-76:34.5	52	4.7	P	31	3.7	P	-	-	-	3.3*	3	I
11:06:05	-76:36.0	130	10.1	PF	140	13.4	PF	300	6.6	P	3.3*	3	I
11:06:35	-77:01.5	330	20.8	PFI	410	27.9	PFI	760	18.8	P	-	-	-
11:06:40	-77:23.5	13*	781.7	PFI	38*	2098.5	P I	69*	3	I	-	-	-
11:06:55	-77:18.0	10*	507.6	PFI	14*	634.9	PFI	8.9*	195.0	P I	-	-	-
11:06:60	-76:32.5	83	6.9	PF	36	3.3	P	-	-	-	-	-	-
11:07:15	-77:00.0	-	-	-	100	7.4	PF	530	18.9	PF	-	-	-
11:07:20	-77:28.0	11*	815.4	PFI	78*	4931.4	P I	210*	4685.8	P I	250*	3	I
11:07:30	-76:46.0	120	8.9	PF	190	16.4	PF	410	9.5	P	-	-	-
11:07:35	-76:02.0	160	8.6	PF	47	3.3	P	-	-	-	-	-	-
11:07:55	-77:07.5	-	-	-	-	-	-	-	-	-	5.3*	2	F
11:07:55	-76:07.5	600	43.1	PFI	560	36.3	PFI	460	7.5	PFI	-	-	-
11:08:25	-77:10.5	100	5.7	PF	130	7.0	PF	540	16.6	PF	-	-	-
11:08:25	-76:19.5	12*	760.2	PFI	30*	1478.7	PFI	97*	1363.8	PFI	294*	2	F
11:08:35	-77:21.0	540	32.6	PFI	500	3-3	FI	-	-	-	-	-	-
11:08:35	-76:13.5	350	21.8	P	4.8*	3	I	-	-	-	-	-	-
11:09:15	-77:16.5	290	17.9	PFI	430	24.0	PFI	830	17.2	PFI	-	-	-
11:09:25	-77:02.0	380	36.3	PFI	740	52.2	PFI	1.1*	27.4	PFI	-	-	-
11:09:25	-76:29.5	-	-	-	67	3.2	PF	-	-	-	-	-	-
11:09:40	-77:10.0	68	5.2	PF	70	4.6	P	810	16.0	P	-	-	-
11:09:45	-77:15.0	170	13.3	PF	-	-	-	-	-	-	5.2*	2	F
11:10:10	-76:04.0	410	27.0	PFI	550	46.1	PFI	550	5.8	PFI	-	-	-
11:10:50	-76:21.0	500	27.3	PFI	310	12.4	PFI	-	-	-	-	-	-
11:10:60	-76:28.5	2.0*	140.8	PFI	2.7*	151.0	PFI	2.5*	29.3	PFI	-	-	-
11:11:15	-77:06.5	34	4.0	P	120	7.1	PF	970	21.4	PFI	4.2*	2-3	FI
11:11:50	-76:10.0	2.4*	175.9	PFI	1000	80.6	PFI	460	4.6	PF	1.9*	2	I
11:11:55	-75:47.0	170	10.2	PF	50	3.3	P	-	-	-	-	-	-
11:12:00	-77:51.0	1.1*	120.3	P I	690	58.1	P I	380	8.5	PF	-	-	-
11:12:05	-77:45.0	70	7.2	PF	34	3.2	P	-	-	-	-	-	-
11:12:30	-76:38.5	1.9*	209.5	PFI	680	59.8	PFI	-	-	-	-	-	-
11:12:40	-76:58.5	160	15.5	PF	46	3.6	P	-	-	-	-	-	-
11:12:45	-77:13.0	92	9.8	PF	-	-	-	420	8.1	PF	-	-	-
11:13:25	-75:42.5	240	14.9	PF	-	-	-	-	-	-	-	-	-
11:13:35	-76:46.0	120	14.8	PF	32	3.0	P	-	-	-	-	-	-
11:13:45	-77:15.0	150	12.9	PF	-	-	-	-	-	-	-	-	-
11:14:20	-76:13.0	310	22.0	PFI	80	5.1	PF	-	-	-	-	-	-
11:14:25	-76:08.5	-	-	-	-	-	-	280	4.5	PF	1.5*	3	I
11:14:25	-76:26.5	-	-	-	51	4.4	P	450	5.0	PFI	-	-	-
11:14:30	-75:57.0	1.1*	124.9	PFI	4.3*	386.9	PFI	42*	479.1	PFI	68*	2-3	FI
11:15:35	-76:58.5	-	-	-	89	5.1	P	490	9.1	PF	-	-	-
11:15:35	-76:37.0	350	26.7	PFI	82	7.1	PF	-	-	-	-	-	-
11:15:55	-76:11.0	970	69.4	PFI	270	18.2	PFI	-	-	-	-	-	-
11:16:00	-76:48.5	100	12.2	PF	220	16.4	PFI	610	8.8	PFI	-	-	-
11:16:15	-76:22.5	-	-	-	70	4.4	P	200	3.6	PF	-	-	-
11:16:35	-77:00.5	290	27.2	PFI	140	7.8	P	580	7.6	PF	-	-	-
11:16:45	-76:25.0	140	6.4	PF	71	5.3	P	-	-	-	-	-	-
11:17:25	-76:53.0	89	2	F	40	3.5	P	-	-	-	-	-	-

Table 6. continued

ra (1950)	dec	F1	SN	C	F2	SN	C	F3	SN	C	F4	SN	C
11:18:15	-76:13.0	690	39.6	PFI	270	17.9	PFI	310	5.1	P	2.3*	3	I
11:18:15	-77:05.0	41	3.1	P	53	3.4	PF	-	-	-	-	-	-
11:19:35	-77:45.5	58	3.2	PF	-	-	-	-	-	-	-	-	-
11:19:55	-76:21.5	260	10.1	P	89	5.7	PF	-	-	-	-	-	-
11:19:60	-77:49.5	82	4.6	PF	81	4.4	P	280	2	F	-	-	-
11:20:20	-77:20.5	170	18.9	PF	81	5.0	P	-	-	-	-	-	-
11:20:30	-75:55.0	430	23.1	PFI	140	10.5	PF	-	-	-	-	-	-
11:21:10	-76:33.0	430	12.7	PFI	130	5.8	P	-	-	-	-	-	-
11:21:20	-76:26.5	22*	624.7	PFI	6.8*	290.7	PFI	1.5*	23.4	PFI	-	-	-
11:21:35	-77:24.0	130	13.7	PF	-	-	-	-	-	-	-	-	-
11:22:05	-76:21.0	-	-	-	57	3.3	P	-	-	-	4.7*	2	F
11:22:20	-76:53.0	72	3.9	P	73	5.5	PF	560	15.5	PFI	-	-	-
11:22:45	-77:44.0	280	16.8	PFI	98	4.6	PF	-	-	-	-	-	-
11:23:00	-76:20.5	250	10.2	PFI	140	8.7	PF	-	-	-	-	-	-
11:23:50	-76:44.0	1.4*	53.0	PFI	470	20.4	PFI	-	-	-	-	-	-
11:23:50	-76:57.0	110	4.7	P	83	5.2	P	200	2	F	-	-	-
11:23:60	-76:14.5	210	12.1	PF	71	3.6	PF	-	-	-	-	-	-
11:24:55	-76:54.0	6.1*	238.6	PFI	3.1*	155.2	PFI	480	2-3	FI	-	-	-
11:26:40	-77:21.5	170	8.6	PF	-	-	-	-	-	-	-	-	-

Table 7. New Source List (NSL). Fluxes are in mJy

ra (1950)	dec	F1	SN	F2	SN	F3	SN
10:34:30	-77:09.0	-	-	70	4.2	-	-
10:34:50	-76:50.5	76	3.5	54	3.1	-	-
10:35:45	-77:01.5	73	4.3	60	3.5	-	-
10:36:00	-77:06.0	86	5.1	50	3.0	-	-
10:36:00	-77:10.0	53	3.1	56	3.4	-	-
10:36:15	-77:12.0	69	4.0	-	-	-	-
10:36:25	-77:00.0	73	4.2	-	-	-	-
10:36:45	-77:08.5	220	13.0	65	4.0	-	-
10:39:05	-77:14.0	110	6.5	41	3.0	-	-
10:39:15	-76:51.5	-	-	46	3.3	250	3.3
10:39:50	-76:44.0	58	4.4	-	-	-	-
10:39:55	-77:14.5	-	-	72	4.2	-	-
10:40:00	-76:49.5	37	3.4	54	4.3	-	-
10:40:20	-76:58.5	61	4.7	48	3.4	-	-
10:40:30	-76:41.5	64	4.4	-	-	-	-
10:41:15	-77:02.0	59	3.9	57	3.8	-	-
10:41:25	-76:59.5	44	3.8	51	3.6	190	3.6
10:41:55	-76:46.5	55	4.3	-	-	200	4.0
10:42:00	-76:48.0	48	4.3	-	-	-	-
10:42:00	-76:53.0	44	4.4	-	-	-	-
10:42:25	-77:05.0	85	5.0	67	4.5	-	-
10:42:45	-76:45.0	56	4.2	-	-	-	-
10:42:55	-77:14.0	52	3.3	70	3.8	-	-
10:43:50	-76:47.0	44	3.4	39	3.0	260	4.7
10:43:55	-76:50.5	110	9.9	-	-	-	-
10:44:05	-76:52.5	110	10.4	-	-	-	-
10:44:05	-77:09.0	57	3.1	59	4.1	830	13.6
10:44:10	-76:43.0	62	4.0	-	-	-	-
10:44:15	-77:05.5	58	3.2	33	3.3	-	-
10:44:30	-76:60.0	150	11.2	52	5.0	-	-

Table 7. continued

ra (1950)	dec	F1	SN	F2	SN	F3	SN
10:45:35	-77:07.0	62	3.7	42	3.8	140	3.5
10:46:25	-77:47.5	-	-	-	-	620	6.3
10:46:25	-76:41.5	100	7.0	-	-	-	-
10:46:35	-77:06.0	45	3.7	35	3.1	-	-
10:46:55	-77:03.5	48	4.0	-	-	-	-
10:47:05	-76:37.5	91	5.6	43	4.3	-	-
10:47:15	-76:40.0	110	7.8	31	3.0	-	-
10:47:20	-77:05.5	49	4.5	37	3.3	-	-
10:47:30	-76:36.0	66	4.2	-	-	-	-
10:48:00	-77:06.0	51	4.4	35	3.1	-	-
10:48:20	-77:33.5	-	-	200	5.9	-	-
10:48:30	-77:37.0	-	-	190	5.2	-	-
10:48:35	-76:52.5	38	4.2	-	-	-	-
10:48:45	-77:31.0	-	-	78	3.2	260	3.6
10:49:05	-77:47.0	57	4.3	-	-	-	-
10:49:15	-77:52.5	-	-	72	4.4	-	-
10:49:20	-77:55.0	-	-	120	6.9	-	-
10:49:35	-77:38.5	64	5.8	140	4.6	-	-
10:49:50	-76:39.0	54	5.1	31	3.5	-	-
10:49:55	-77:41.5	100	9.7	120	5.0	-	-
10:49:60	-77:36.0	95	8.7	-	-	260	3.6
10:50:05	-77:53.5	42	3.4	54	4.0	-	-
10:50:05	-76:35.5	35	3.5	34	3.9	-	-
10:50:15	-77:02.5	40	4.5	-	-	-	-
10:50:20	-77:44.5	86	8.3	130	6.8	-	-
10:50:30	-76:53.5	26	3.4	40	4.0	-	-
10:50:40	-77:20.0	74	4.3	-	-	-	-
10:50:50	-77:11.0	94	8.0	-	-	-	-
10:50:55	-77:34.5	-	-	120	5.6	-	-
10:51:05	-76:30.0	79	4.4	64	4.9	-	-
10:51:10	-76:36.0	46	4.1	-	-	-	-
10:51:25	-76:44.0	32	4.0	-	-	-	-
10:51:25	-77:01.5	27	3.3	40	3.5	120	3.2
10:51:25	-77:39.0	-	-	93	6.8	-	-
10:51:30	-78:03.0	55	5.0	-	-	-	-
10:51:45	-77:36.5	-	-	64	4.3	-	-
10:51:45	-77:57.0	110	10.0	41	3.2	-	-
10:51:55	-76:35.5	48	3.8	67	5.3	-	-
10:51:60	-76:32.0	-	-	77	4.9	-	-
10:51:60	-77:33.5	-	-	37	3.0	210	3.7
10:52:00	-77:09.0	-	-	74	5.5	-	-
10:52:10	-78:05.5	58	5.5	-	-	-	-
10:52:20	-77:10.5	51	4.4	-	-	-	-
10:52:60	-77:05.0	35	3.7	38	3.1	-	-
10:53:05	-77:54.5	40	3.6	48	4.1	-	-
10:53:05	-77:08.0	52	4.6	43	3.1	-	-
10:53:15	-78:09.5	47	4.4	-	-	-	-
10:53:15	-77:14.0	54	4.9	230	17.3	-	-
10:53:40	-77:45.5	33	3.1	34	3.0	-	-
10:53:40	-77:17.5	56	4.9	-	-	-	-
10:53:55	-78:10.5	-	-	73	4.5	-	-
10:54:00	-77:01.0	48	4.4	45	3.4	-	-
10:54:05	-77:13.5	34	3.7	65	5.2	-	-
10:54:20	-77:60.0	38	3.4	39	3.2	-	-
10:54:40	-76:19.5	68	4.4	-	-	220	3.9
10:55:20	-76:45.0	-	-	53	4.0	-	-
10:55:40	-76:22.0	60	4.1	-	-	-	-
10:55:50	-76:20.0	78	5.2	-	-	-	-

ra (1950)	dec	F1	SN	F2	SN	F3	SN
10:56:05	-77:09.0	58	6.6	36	3.8	-	-
10:56:25	-77:06.0	41	5.0	-	-	-	-
10:56:50	-77:12.5	59	8.3	-	-	-	-
10:57:40	-77:25.0	39	4.9	-	-	-	-
10:57:40	-78:10.5	42	3.2	54	3.3	-	-
10:57:45	-77:22.0	31	4.8	-	-	-	-
10:57:50	-77:15.5	27	4.3	-	-	-	-
10:58:10	-77:37.0	41	3.1	43	3.4	-	-
10:58:55	-77:57.5	49	3.9	54	5.0	-	-
10:59:00	-78:00.5	-	-	50	4.3	-	-
10:59:05	-76:19.0	31	3.0	-	-	210	5.1
10:59:10	-77:54.0	46	3.7	32	3.5	-	-
10:59:20	-77:34.5	37	3.3	50	3.5	-	-
10:59:35	-77:36.5	-	-	54	4.1	-	-
10:59:45	-77:57.5	53	3.7	48	4.5	-	-
10:59:55	-78:08.0	66	4.4	53	3.8	-	-
11:00:05	-77:20.0	32	4.9	-	-	-	-
11:00:15	-77:07.0	-	-	34	4.1	-	-
11:00:40	-77:53.0	37	3.1	28	3.3	-	-
11:00:40	-76:21.0	70	8.9	39	3.7	260	7.6
11:01:10	-76:16.0	56	5.9	-	-	-	-
11:01:15	-76:34.5	27	4.2	-	-	-	-
11:01:40	-76:59.5	-	-	35	6.2	-	-
11:01:45	-77:05.5	69	6.8	51	5.4	-	-
11:01:50	-76:47.5	-	-	75	5.0	-	-
11:01:55	-76:56.0	-	-	59	7.4	-	-
11:02:05	-77:07.5	-	-	38	4.1	-	-
11:02:20	-76:25.5	39	5.7	24	3.1	-	-
11:02:25	-78:05.5	63	5.0	48	3.6	-	-
11:02:30	-76:17.0	-	-	-	-	410	13.4
11:02:35	-76:44.5	72	6.4	-	-	-	-
11:02:40	-77:05.5	-	-	50	4.8	-	-
11:03:05	-78:06.5	49	4.5	-	-	-	-
11:03:05	-77:37.5	-	-	160	13.4	-	-
11:03:05	-77:21.0	-	-	48	4.0	-	-
11:03:10	-77:10.5	30	4.2	-	-	-	-
11:03:15	-76:09.0	48	4.2	-	-	-	-
11:03:15	-78:03.0	42	4.0	56	3.9	-	-
11:03:20	-76:45.0	40	4.0	-	-	-	-
11:04:20	-76:53.5	-	-	54	4.8	-	-
11:04:40	-76:40.0	37	4.0	26	3.4	300	6.7
11:04:40	-76:10.0	-	-	-	-	280	7.5
11:04:50	-77:24.0	60	5.6	-	-	-	-
11:05:10	-78:04.5	71	5.5	63	4.1	-	-
11:05:15	-76:19.5	150	11.3	130	8.5	340	8.5
11:05:20	-78:01.5	47	4.1	51	3.6	-	-
11:05:25	-77:34.5	39	4.1	-	-	-	-
11:05:40	-77:03.0	120	7.5	-	-	-	-
11:05:50	-76:41.0	-	-	-	-	280	6.2
11:05:60	-78:04.0	35	3.2	53	3.7	-	-
11:06:00	-76:18.5	-	-	57	4.0	-	-
11:06:05	-76:53.0	40	3.2	34	3.2	390	7.6
11:06:15	-77:45.0	58	5.1	-	-	-	-
11:06:45	-76:25.0	40	3.0	68	4.4	-	-
11:06:50	-77:54.5	37	3.3	46	4.0	-	-
11:06:55	-76:08.0	-	-	-	-	210	4.4
11:06:55	-78:03.0	57	4.1	-	-	-	-
11:07:00	-78:00.5	49	4.0	-	-	-	-

Table 7. continued

ra (1950)	dec	F1	SN	F2	SN	F3	SN
11:07:25	-77:52.0	38	3.4	48	4.8	-	-
11:07:30	-76:48.5	61	5.3	-	-	-	-
11:07:50	-76:39.5	-	-	-	-	470	9.4
11:07:60	-77:49.0	50	4.8	-	-	-	-
11:08:05	-77:14.0	60	4.8	-	-	-	-
11:08:25	-76:42.5	38	4.5	-	-	-	-
11:08:25	-76:40.0	35	4.0	29	3.3	-	-
11:09:05	-77:20.0	-	-	250	13.0	-	-
11:09:10	-76:58.0	-	-	110	8.4	-	-
11:09:10	-76:45.0	-	-	-	-	420	8.6
11:09:35	-77:45.0	63	7.3	-	-	-	-
11:09:40	-75:55.0	45	3.7	51	4.2	-	-
11:10:00	-77:12.0	45	5.3	-	-	-	-
11:10:25	-76:39.0	27	3.1	37	3.1	-	-
11:10:30	-78:01.0	-	-	87	6.3	-	-
11:10:35	-75:59.0	130	10.7	-	-	-	-
11:11:10	-78:01.0	84	5.7	-	-	-	-
11:11:10	-77:01.0	35	3.4	36	3.6	-	-
11:11:15	-77:18.0	33	4.6	-	-	690	11.5
11:11:25	-77:56.5	89	7.0	35	3.1	-	-
11:11:30	-77:38.0	-	-	39	4.1	-	-
11:11:55	-78:00.0	130	8.9	-	-	-	-
11:12:05	-76:51.5	-	-	30	3.4	510	7.8
11:12:55	-77:16.5	50	5.2	-	-	-	-
11:13:05	-77:07.0	-	-	77	4.7	-	-
11:13:25	-76:01.5	24	3.1	23	3.2	-	-
11:13:30	-77:54.5	52	4.6	40	3.3	-	-
11:13:60	-77:24.5	-	-	60	4.9	-	-
11:14:20	-77:56.0	33	3.2	80	6.0	-	-
11:14:25	-75:49.0	80	5.2	35	3.0	-	-
11:14:35	-77:37.5	55	6.4	-	-	-	-
11:14:40	-75:47.0	99	4.8	-	-	-	-
11:14:45	-77:58.5	43	3.0	38	3.1	-	-
11:14:60	-77:40.0	39	4.1	-	-	-	-
11:15:10	-76:39.5	38	4.0	-	-	-	-
11:15:15	-77:53.5	45	3.7	36	3.3	-	-
11:15:25	-75:45.0	150	7.0	-	-	-	-
11:15:40	-75:56.5	82	7.8	-	-	-	-
11:15:40	-77:56.0	57	4.7	50	3.5	-	-
11:15:60	-77:48.0	42	4.0	-	-	-	-
11:16:05	-75:45.0	89	4.1	-	-	-	-
11:16:30	-76:45.0	36	4.3	33	3.3	-	-
11:16:30	-77:52.0	58	5.1	59	4.4	-	-
11:16:40	-75:42.5	230	9.5	-	-	-	-
11:16:40	-77:54.5	-	-	59	4.1	-	-
11:16:45	-76:51.0	56	5.8	-	-	-	-
11:16:50	-77:42.5	38	3.7	37	3.4	-	-
11:17:05	-76:28.5	-	-	49	5.1	-	-
11:17:05	-76:10.0	-	-	-	-	300	5.0
11:17:10	-76:46.5	53	5.3	-	-	-	-
11:17:10	-76:58.5	-	-	83	5.1	-	-
11:17:10	-76:01.5	50	4.4	-	-	-	-
11:17:20	-77:52.5	73	6.1	44	3.3	-	-
11:17:25	-76:31.5	63	3.6	33	4.3	-	-
11:17:30	-77:48.5	76	6.0	55	3.8	-	-
11:17:40	-76:27.0	-	-	55	4.2	-	-
11:17:40	-77:56.5	74	5.7	45	3.3	-	-
11:17:45	-77:23.0	39	3.9	54	3.6	-	-
11:17:55	-76:52.5	-	-	50	4.3	-	-
11:17:55	-76:29.0	-	-	51	4.1	-	-
11:17:55	-76:38.5	-	-	46	4.3	-	-
11:18:05	-77:50.5	87	6.9	-	-	-	-
11:18:15	-75:39.0	-	-	110	8.8	-	-
11:18:15	-77:53.0	81	6.0	-	-	-	-
11:18:15	-76:08.0	55	3.5	52	3.4	-	-
11:18:20	-76:32.5	73	4.1	47	3.5	-	-
11:18:20	-76:41.0	-	-	53	4.8	-	-
11:18:30	-75:50.0	60	3.8	48	4.6	-	-
11:18:35	-76:37.0	44	3.5	33	3.3	-	-
11:18:35	-77:03.0	39	3.0	69	4.8	-	-
11:18:40	-75:47.5	-	-	41	4.1	-	-
11:18:40	-75:55.5	-	-	70	6.0	-	-
11:18:40	-77:21.5	-	-	73	4.3	-	-
11:18:50	-76:54.0	-	-	62	4.6	-	-
11:18:60	-76:20.5	59	3.3	77	4.4	-	-
11:19:05	-76:11.0	97	5.2	49	3.0	-	-
11:19:05	-76:27.0	-	-	64	4.3	-	-
11:19:05	-76:33.5	-	-	57	4.4	-	-
11:19:05	-77:33.5	58	4.7	-	-	-	-
11:19:05	-76:30.5	110	4.5	64	4.5	-	-
11:19:10	-76:13.5	100	5.2	-	-	-	-
11:19:10	-77:51.5	53	3.7	49	3.1	-	-
11:19:10	-76:55.5	-	-	57	4.9	-	-
11:19:15	-75:52.5	180	10.5	-	-	-	-
11:19:15	-77:35.5	97	7.6	-	-	-	-
11:19:30	-76:58.5	63	4.6	-	-	-	-
11:19:30	-77:03.5	-	-	53	4.1	-	-
11:19:40	-75:49.5	87	4.3	49	4.9	-	-
11:19:40	-77:39.5	82	5.9	-	-	-	-
11:19:40	-77:43.0	120	8.2	51	3.2	-	-
11:19:40	-77:06.0	-	-	60	4.4	-	-
11:19:45	-75:54.0	-	-	54	4.7	-	-
11:19:50	-77:55.0	76	4.8	-	-	-	-
11:19:60	-75:51.0	-	-	45	4.2	-	-
11:20:05	-76:30.0	150	5.0	75	3.8	-	-
11:20:15	-77:47.0	78	4.7	70	3.6	-	-
11:20:20	-76:27.5	-	-	81	4.0	-	-
11:20:25	-77:03.5	51	3.6	79	6.3	-	-
11:20:35	-77:00.5	48	3.2	41	3.8	-	-
11:20:60	-76:46.0	75	4.1	-	-	-	-
11:21:10	-77:50.5	93	5.4	73	3.4	-	-
11:21:10	-76:39.5	89	3.9	43	3.4	-	-
11:21:20	-76:42.0	85	4.0	-	-	-	-
11:21:25	-77:19.5	-	-	88	5.2	-	-
11:21:25	-76:53.5	92	5.1	32	3.1	-	-
11:21:25	-77:53.0	97	5.5	-	-	-	-
11:21:35	-76:02.0	45	3.1	55	3.5	-	-
11:21:40	-77:01.5	-	-	44	4.0	-	-
11:21:55	-76:59.5	66	4.1	-	-	-	-
11:22:05	-76:34.0	-	-	120	4.7	-	-
11:22:05	-77:45.5	45	3.0	88	4.3	-	-
11:22:05	-77:48.5	57	3.5	76	3.9	-	-
11:22:10	-76:23.0	-	-	74	3.8	670	10.0
11:22:10	-76:46.0	68	4.1	-	-	-	-
11:22:10	-77:16.5	-	-	100	5.7	-	-
11:22:15	-77:25.5	37	3.4	57	3.4	-	-

Table 7. continued

ra (1950)	dec	F1	SN	F2	SN	F3	SN
11:22:15	-77:20.5	48	4.8	-	-	-	-
11:22:25	-77:51.0	-	-	93	4.3	-	-
11:22:25	-76:50.0	79	4.0	37	3.4	-	-
11:22:35	-76:58.0	71	4.0	42	3.8	-	-
11:22:40	-77:29.0	58	5.1	-	-	-	-
11:22:55	-77:18.0	-	-	110	6.4	-	-
11:22:55	-76:47.5	-	-	69	4.6	-	-
11:22:55	-76:03.0	-	-	65	4.1	-	-
11:22:60	-76:28.5	140	3.7	130	5.7	-	-
11:23:15	-76:23.0	190	5.4	120	6.3	-	-
11:23:15	-76:59.0	61	3.3	38	3.4	-	-
11:23:20	-77:50.5	100	5.3	170	7.5	-	-
11:23:25	-76:11.5	58	4.0	-	-	-	-
11:23:35	-76:54.5	100	4.3	82	6.2	-	-
11:23:35	-77:15.0	-	-	160	11.1	-	-
11:23:40	-77:48.5	71	4.2	-	-	-	-
11:23:45	-76:01.5	51	4.0	-	-	-	-
11:23:55	-77:25.5	59	4.7	-	-	-	-
11:23:55	-77:01.0	-	-	60	4.7	-	-
11:23:60	-77:51.0	170	9.0	-	-	-	-
11:24:05	-76:47.0	-	-	420	23.3	-	-
11:24:05	-77:40.0	48	3.5	73	4.1	-	-
11:24:15	-77:18.5	52	4.3	-	-	-	-
11:24:50	-77:12.5	49	3.7	200	15.1	-	-
11:24:50	-77:00.5	-	-	57	4.3	-	-
11:25:05	-76:20.0	70	3.1	63	3.5	-	-
11:25:05	-77:16.0	61	4.5	-	-	-	-
11:25:10	-76:16.5	81	4.2	-	-	-	-
11:25:20	-76:12.5	66	4.9	-	-	-	-
11:26:10	-77:18.5	130	8.5	-	-	-	-
11:26:20	-77:34.5	49	3.4	62	3.0	-	-
11:26:30	-77:27.5	77	4.8	-	-	-	-
11:26:35	-77:44.0	80	4.4	-	-	-	-
11:26:45	-77:46.0	77	4.1	-	-	-	-
11:26:55	-77:23.5	140	7.0	-	-	-	-

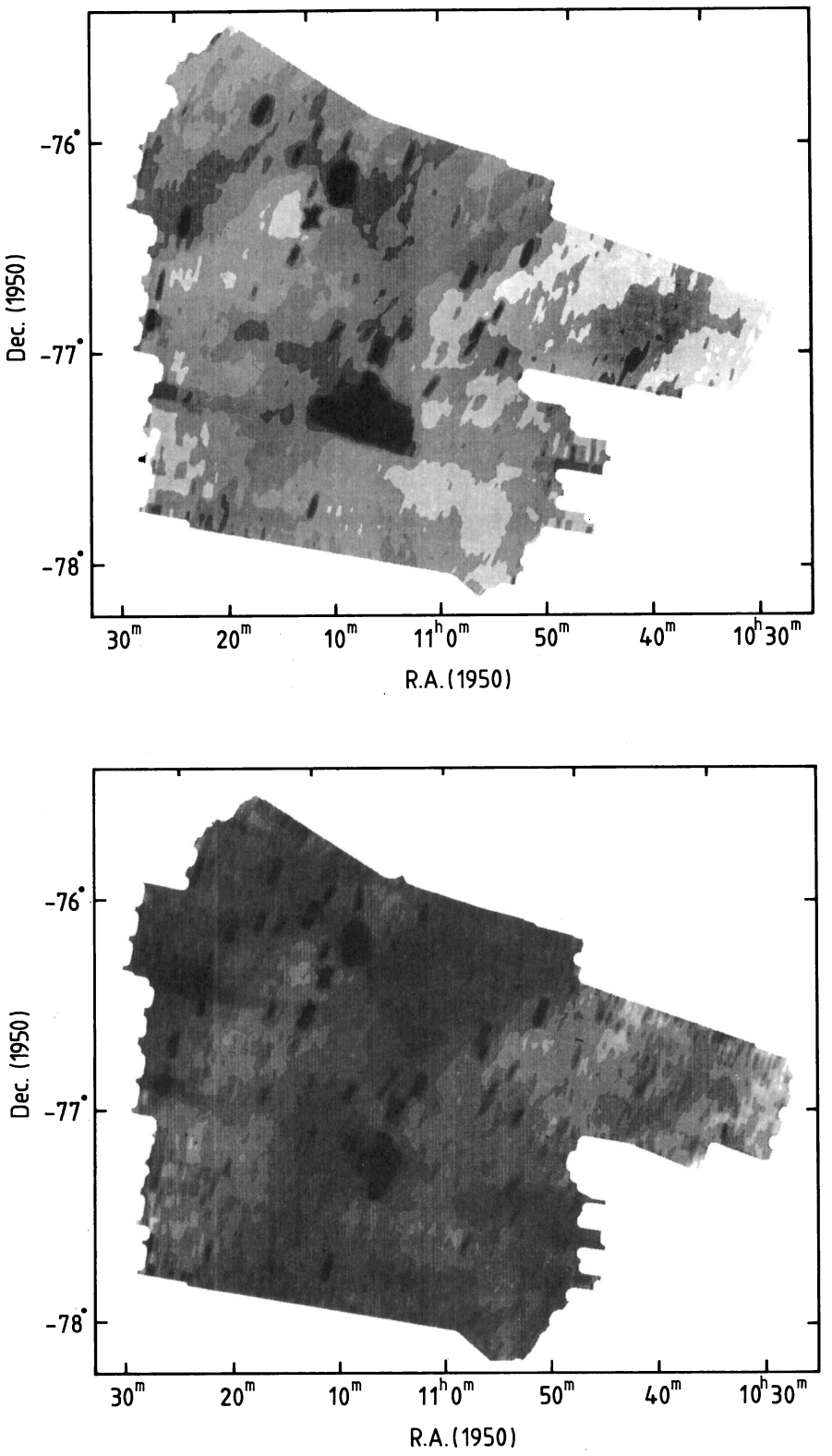

Fig. 7. 12 (left top), 25 (left bottom), 60 (right top), and 100 (right bottom) μm images of coadded PO's. The grayscales are for all images: 0.1, 0.2, 0.3, 0.4, 0.5, 0.7, 0.9, 1.1, 1.3, 1.5, 2, 5, 10, 20, 50, 90 % of the total intensity range (see Table 2)

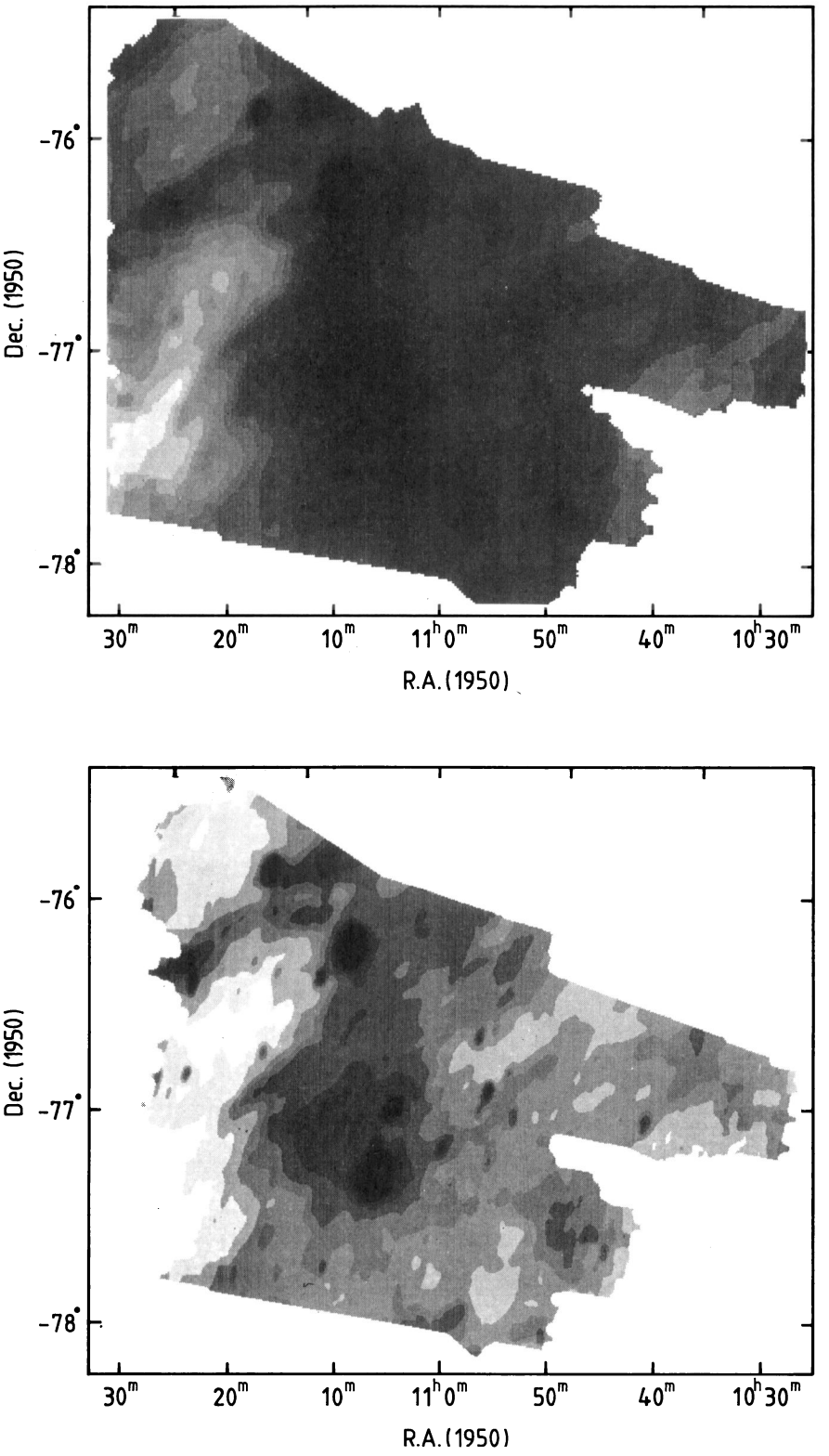

Fig. 7. continued

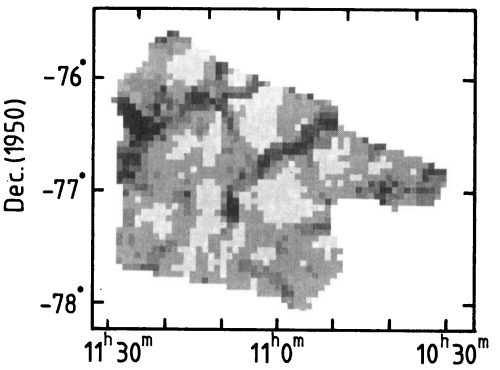

Fig. 8. 12 μm noisemap. The grayscales are -0.1 -0.05 0 0.05 0.1 0.15 0.2 0.25 0.3 0.35 MJy/sterad